Sugiawati et al. Nanoscale Research Letters (2016) 11:365
DOI 10.1186/s11671-016-1574-7

Nanoscale Research Letters

NANO EXPRESS Open Access

Porous NASICON-Type $Li_3Fe_2(PO_4)_3$ Thin Film Deposited by RF Sputtering as Cathode Material for Li-Ion Microbatteries

Vinsensia Ade Sugiawati[1], Florence Vacandio[1*], Marielle Eyraud[1], Philippe Knauth[1] and Thierry Djenizian[1,2*]

Abstract

We report the electrochemical performance of porous NASICON-type $Li_3Fe_2(PO_4)_3$ thin films to be used as a cathode for Li-ion microbatteries. Crystalline porous NASICON-type $Li_3Fe_2(PO_4)_3$ layers were obtained by radio frequency sputtering with an annealing treatment. The thin films were characterized by XRD, SEM, and electrochemical techniques. The chronoamperometry experiments showed that a discharge capacity of 88 $mAhg^{-1}$ (23 $\mu Ahcm^{-2}$) is attained for the first cycle at C/10 to reach 65 $mAhg^{-1}$ (17 $\mu Ahcm^{-2}$) after 10 cycles with a good stability over 40 cycles.

Keywords: Radio frequency sputtering, Li-ion microbatteries, NASICON-type $Li_3Fe_2(PO_4)_3$, Cathode thin film

Background

Due to remarkable properties such as excellent cycle life, high thermal resistance, no memory effect, and low self-discharge, Li-ion batteries have attracted great attention in electrochemical energy storage [1–3]. More recently, the miniaturization of these power sources has been investigated to meet many applications in microelectronics such as real-time clocking (RTC), radio frequency identification (RFID), sensors, medical implants, memory backup power, solar cell, and smartcards [4–6]. One of the major challenges in the microbattery field is related to the manufacturing process and its compatibility with the integrated circuit technology. Particularly, metallic Li which is currently used as a negative electrode is not compatible with the reflow soldering process because of its low melting point (180.5 °C). Therefore, the rocking chair technology involving stable materials must be explored. Many researches focused on the development of new components with nanostructured materials and 3D designs [7–11].

As potential cathode materials, the NASICON-type compounds $A_3Fe_2(XO_4)_3$ (A = Li, Na; X = P, As, S) with 3D frameworks like $Li_3Fe_2(PO_4)_3$ have attracted considerable attention [12]. NASICON-type $Li_3Fe_2(PO_4)_3$ can generate 2.8 V vs. Li with an excellent capacity retention, and up to 2 mol of Li^+ can be reversibly intercalated into $Li_3Fe_2(PO_4)_3$, delivering a capacity of 128 $mAhg^{-1}$. NASICON has also a relatively high ionic conductivity resulting from the disorder of lithium ions in the structure, favorable redox properties, low cost, structural stability, and simple fabrication procedures [5, 6, 12]. Many methods have been reported to synthesize $Li_3Fe_2(PO_4)_3$ nanostructures such as hydrothermal [13, 14], gel combustion [15], solid state [16–19], solution with the use of citric acid [20], sol-gel [21], ultrasonic spray combustion [22], and ion exchange with molten salt [23, 24].

In this work, we report the fabrication of porous NASICON-type $Li_3Fe_2(PO_4)_3$ thin film electrodes by radio frequency sputtering. Sputtering techniques are widely employed in microelectronics for the successive deposition of thin films; they are the main process used to fabricate planar all-solid-state Li-ion microbatteries [25, 26]. To the best of our knowledge, this approach has never been applied to deposit $Li_3Fe_2(PO_4)_3$. We show that this material tested as a cathode reveals a good electrochemical behavior for all-solid-state Li-ion microbatteries.

* Correspondence: florence.vacandio@univ-amu.fr; thierry.djenizian@univ-amu.fr
[1]Aix-Marseille University, CNRS, MADIRELLaboratory, UMR 7246, 13397 Marseille, France
Full list of author information is available at the end of the article

Methods

Preparation of $Li_3Fe_2(PO_4)_3$ Thin Films

Firstly, thin films of $LiFePO_4$ were deposited on titanium foil as substrate by radio frequency (RF) sputtering (PLASSYS). The target was $LiFePO_4$ (purity 99.9 %, Neyco). The process was carried out in a vacuum chamber with a base pressure before deposition of 10^{-6} Torr. The sputtering gas was pure argon, and the working pressure was 10 mTorr with a gas flow of 21.5 sccm. A sputtering power of 150 W was applied to the target. The deposition time was 3 h. Secondly, the as-deposited thin films were annealed in air at 700 °C for 3 h with a heating rate of 10 °C min^{-1} (furnace: NABERTHERM Controller B 180).

Structural Characterization

Phases and crystallinity of thin films were examined by X-ray diffraction (XRD) with Cu Kα radiation (wavelength = 1.5405 Å) using a D5000 BRUKER-SIEMENS diffractometer. The morphology of the $Li_3Fe_2(PO_4)_3$ was investigated by scanning electron microscopy (SEM, Hitachi, S-570). Thickness measurement was performed by profilometry analysis using a DEKTAT XT (BRUKER) equipment. A portion of the sample is masked during deposition, and the thickness is given by the height of the step.

Electrochemical Measurements

The electrochemical tests of the half-cell were performed using Swagelok cell assembled in a glove box filled with purified argon in which moisture and oxygen content were less than 0.5 ppm. The half-cells consisted of metallic Li as counter electrode. Two circular sheets of Whatman glass microfiber soaked with lithium hexafluorophosphate in ethylene carbonate and diethylene carbonate (1 M $LiPF_6$ in (EC:DEC) 1:1 *w*/*w*) were used as separator. Cyclic voltammetry measurements were performed using a Versastat potentiostat (AMETEK) in the range of 1.25–5 V vs. Li/Li^+ with a scan rate of 1 mVs^{-1}. Galvanostatic cycles were performed with a VMP3 (Bio Logic) at 25 °C between 2 and 4 V vs. Li/Li^+. The different cycles of the charge/discharge rate were investigated at a kinetic rate of C/10 and C/5 considering that the theoretical capacity of $Li_3Fe_2(PO_4)_3$ is 128.25 $mAhg^{-1}$. Hence, the applied currents were 3.3 and 6.6 μA cm^{-2}, respectively. No additives or binder was used for all electrochemical tests.

Results and Discussion

Prior to battery assembly, the crystallinity of the thin films were examined by XRD. The XRD patterns of initial target and as-deposited sample are shown in Fig. 1. It can be seen that the target is well-crystallized and corresponds to the Olivine-type $LiFePO_4$ phase (JCPDS file no. 040-1499). Various deposition parameters (such as target power, substrate temperature, or argon pressure) were previously investigated, and in all cases, the as-deposited thin films were amorphous. As it can be seen in Fig. 1, the annealing treatment leads to the crystallization of NASICON-type $Li_3Fe_2(PO_4)_2$ phases (JCPDS file no. 047-0107), which is known to have better electrochemical properties [27]. Three small peaks are attributable to the Fe_2O_3 phase. The oxidation state of Fe in $LiFePO_4$ and $Li_3Fe_2(PO_4)$ are +II and +III, respectively. It can be noted that the annealing in air of amorphous $LiFePO_4$ not only leads to crystallization but also to the iron oxidation according to (Eq. 1) [28, 29]:

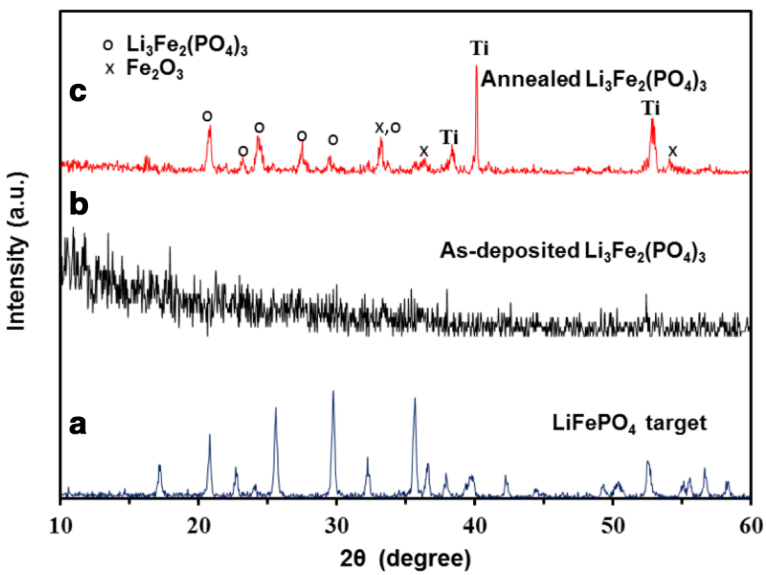

Fig. 1 XRD patterns of samples **a** $LiFePO_4$ target, **b** as-deposited $Li_3Fe_2(PO_4)_3$, and **c** annealed $Li_3Fe_2(PO_4)_3$ at 700 °C for 3 h

$$12LiFePO_4 + 3O_2 = 4Li_3Fe_2(PO_4)_3 + 2Fe_2O_3 \quad (1)$$

However, the conversion reaction of Fe_2O_3 with Li^+ occurs at low potential which is not interesting for its use as a cathode [30, 31].

The morphology of the $Li_3Fe_2(PO_4)_3$ thin films before and after annealing was observed by SEM. From Fig. 2a, it is apparent that the as-deposited $Li_3Fe_2(PO_4)_3$ layer is homogeneous with a thickness of 850 nm according to the surface profilometry analysis given in Fig. 2b. After annealing, the film became rough and a sponge-like texture clearly appeared (Fig. 2c, d). Hence, the thermal treatment promoted the formation of a mesoporous material with a larger surface area than the as-deposited layer.

The electrochemical characterization of the porous $Li_3Fe_2(PO_4)_3$ thin film was carried out by cyclic voltammetry (CV). Figure 3 shows the cyclic voltammogram (CV) is obtained. In agreement with literature, the electrochemical reactivity of crystalline $Li_3Fe_2(PO_4)_3$ is confirmed by the presence of anodic and cathodic peaks [3, 32]. These two peak pairs can be attributed to the reversible insertion reactions of two Li^+ according to Eqs. (2) and (3):

- First reduction (R1 2.68 V/Li) and oxidation peaks (O1 2.58 V/Li)

$$Li_4Fe_2(PO_4)_3 = Li^+ + Li_3Fe_2(PO_4)_3 + e^- \quad (2)$$

- Second reduction (R2 2.72 V/Li) and oxidation peaks (O2 2.85 V/Li)

$$Li_5Fe_2(PO_4)_3 = Li^+ + Li_4Fe_2(PO_4)_3 + e^- \quad (3)$$

The presence of an additional reversible peak (O3 and R3 peaks) at around 2.4 V reveals that Li^+ can also react with another phase. This active material is supposed to be $LiFePO_4(OH)$ into which lithium intercalation occurs through the reduction of Fe^{3+} to Fe^{2+} [33–35].

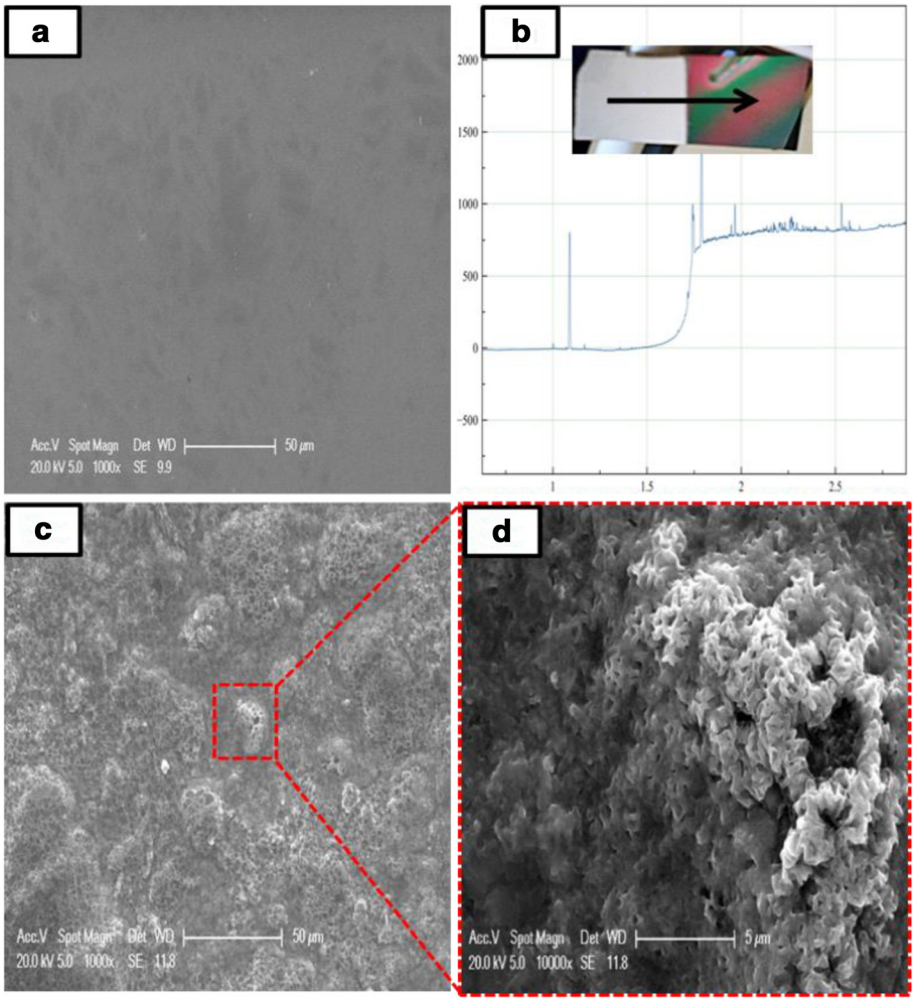

Fig. 2 **a** as-deposited $Li_3Fe_2(PO_4)_3$ with **b** profilometry analysis, low (**c**) and high magnification (**d**) SEM images of porous $Li_3Fe_2(PO_4)_3$ deposited by RF sputtering after annealing treatment

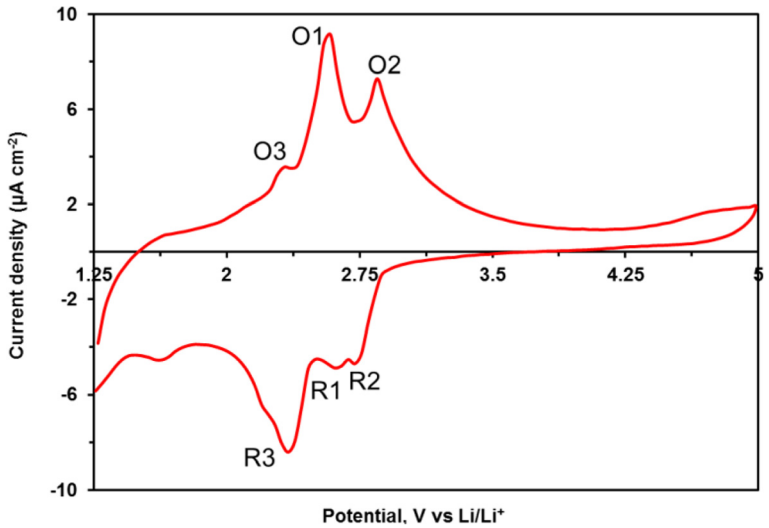

Fig. 3 CV curve of the annealed $Li_3Fe_2(PO_4)_3$ thin film deposited on Ti substrate recorded at a scan rate of 1 mVs^{-1}

Compared with literature, it can be noticed that the peaks are quite broad. This phenomenon can be explained by the presence of pores. Indeed, the large surface area offered by the porous texture promotes the storage of charge at the surface according to a non-faradaic process. Hence, the contribution of the capacitive effect leads to the broadening of the peaks.

The galvanostatic charge/discharge profiles obtained at C/10 of the half-cell battery are shown in Fig. 4a. In agreement with the CV curve, the presence of three pseudo-plateaus confirms that Li^+ ions react with $Li_3Fe_2(PO_4)_3$ and $LiFePO_4(OH)$.

The capacity values obtained for the as-deposited sample (Fig. 4b) are very low in the range of 1–2 $\mu Ahcm^{-2}$. But, a first discharge capacity of 88 $mAhg^{-1}$ (23 $\mu Ahcm^{-2}$) is achieved at C/10 for the annealed sample. An average value of about 65 $mAhg^{-1}$ (17 $\mu Ahcm^{-2}$) is delivered after 20 cycles. This capacity corresponds to more than 50 % of the theoretical capacity of $Li_3Fe_2(PO_4)_3$ (33 $\mu Ahcm^{-2}$). We can observe that capacity is slightly fading during the first cycles. The capacity lost may be caused by the different effects which are associated with side reactions due to the phase changes in the insertion electrode, dissolution of the active material, or the decomposition of the electrolyte. The capacity loss has been also discussed by Song et al. [36] who reported that capacity fading can be attributed to surface impurities (such as lithiated iron oxide which is also involved in the lithium insertion/extraction) leading to the irreversible reaction of Li^+ with iron oxide and the formation of a solid electrolyte interface (SEI) at the surface of the electrode.

In order to study the operational stability of the NASICON-type $Li_3Fe_2(PO_4)_3$, the cycling life performance has been also studied at two different C-rates (Fig. 4b). From this graph, it can be seen that the capacity becomes stable after 10 cycles. At C/5, the battery capacity is about 50 $mAhg^{-1}$ (13 $\mu Ahcm^{-2}$) and remains constant over 40 cycles. These results also show that the

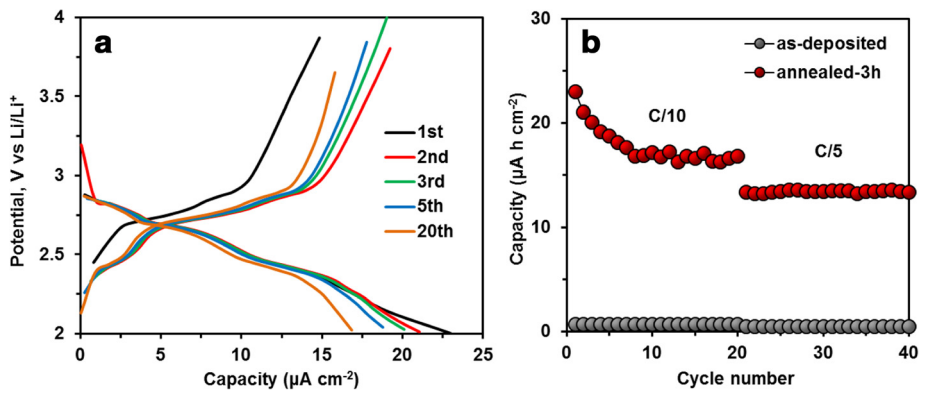

Fig. 4 Battery cycling tests at the kinetic rate of C/10 in the potential window of 2–4 V (**a**). Discharge capacity of cathode at multi-C-rate (**b**)

porous geometry of the mesoporous electrode is beneficial for tolerating the volume expansion that generally occur during alloying/de-alloying reactions.

Conclusions

In this work, we report the fabrication of mesoporous NASICON-type $Li_3Fe_2(PO_4)_3$ thin film by radio frequency sputtering. The electrochemical studies suggest that after annealing, the crystallized layer is also composed of $LiFePO_4(OH)$, which is able to react reversibly with Li^+. In the first cycle, the discharge capacity reaches about 88 $mAhg^{-1}$ (23 $\mu Ahcm^{-2}$) at C/10 and attains 65 $mAhg^{-1}$ (17 $\mu Ahcm^{-2}$) after 10 cycles. The electrochemical characterizations also reveal a good stability suggesting that this material can be used as a cathode for Li-ion microbatteries.

Acknowledgements
This work has been carried out thanks to the support of the A*MIDEX project (*no. ANR-11-IDEX-0001-02*) funded by the "Investissements d'Avenir" French government program, managed by the French National Research Agency (ANR).

Authors' contributions
VAS did experimental works. ME and PK participated to the discussion. FV and TD supervised the research work.

Competing Interests
The authors declare that they have no competing interests.

Author details
[1]Aix-Marseille University, CNRS, MADIRELLaboratory, UMR 7246, 13397 Marseille, France. [2]Department of Flexible Electronics, Ecole National Supérieure des Mines de Saint-Etienne, Center of Microelectronics in Provence, 13 541 Gardanne, France.

Received: 3 May 2016
Published online: 17 August 2016

References

1. Padhi AK, Nanjundaswamy KS, Goodenough JB (1997) Phospho-olivines as positive-electrode materials for rechargeable lithium batteries. J Electrochem Soc 144:1188–1194
2. Li D, Zhou H (2014) Two-phase transition of Li-intercalation compounds in Li-ion batteries. Mater Today 17:451–463
3. Xu J, Deshpande RD, Pan J et al (2015) Electrode side reactions, capacity loss and mechanical degradation in lithium-ion batteries. J Electrochem Soc 162:A2026–A2035
4. Porthault H, Decaux C (2016) Electrodeposition of lithium metal thin films and its application in all-solid-state microbatteries. Electrochim Acta 194:330–337
5. Luais E, Ghamouss F, Wolfman J et al (2015) Mesoporous silicon negative electrode for thin film lithium-ion microbatteries. J Power Sources 274:693–700
6. Lafont U, Anastasopol A, Garcia-Tamayo E, Kelder E (2012) Electrostatic spray pyrolysis of $LiNi_{0.5}Mn_{1.5}O_4$ films for 3D Li-ion microbatteries. Thin Solid Films 520:3464–3471
7. Ferrari S, Loveridge M, Beattie SD et al (2015) Latest advances in the manufacturing of 3D rechargeable lithium microbatteries. J Power Sources 286:25–46
8. Meng X, Yang X-Q, Sun X (2012) Emerging applications of atomic layer deposition for lithium-ion battery studies. Adv Mater 24:3589–3615
9. Plylahan N, Kyerematen N, Eyraud M et al (2012) Highly conformal electrodeposition of copolymer electrolytes into titania nanotubes for 3D Li-ion batteries. Nanoscale Res Lett 7:349
10. Plylahan N, Maria S, Phan TN et al (2014) Enhanced electrochemical performance of lithium-ion batteries by conformal coating of polymer electrolyte. Nanoscale Res Lett 9:544
11. Ellis BL, Knauth P, Djenizian T (2014) Three-dimensional self-supported metal oxides for advanced energy storage. Adv Mater 26:3368–3397
12. Masquelier C, Padhi AK, Nanjundaswamy KS, Goodenough JB (1998) New cathode materials for rechargeable lithium batteries: the 3-D framework structures $Li_3Fe_2(XO_4)_3$(X = P, As). J Solid State Chem 135:228–234
13. Sato M (2002) Preparation of iron phosphate cathode material of $Li_3Fe_2(PO_4)_3$ by hydrothermal reaction and thermal decomposition processes. Solid State Ionics 152–153:247–251
14. Yang S, Zavalij PY, Stanley Whittingham M (2001) Hydrothermal synthesis of lithium iron phosphate cathodes. Electrochem Commun 3:505–508
15. Karami H, Taala F (2011) Synthesis, characterization and application of $Li_3Fe_2(PO_4)_3$ nanoparticles as cathode of lithium-ion rechargeable batteries. J Power Sources 196:6400–6411
16. Morcrette M, Wurm C, Masquelier C (2002) On the way to the optimization of $Li_3Fe_2(PO_4)_3$ positive electrode materials. Solid State Sci 4:239–246
17. Pylinina AI, Mikhalenko II, Ivanov-Shits AK et al (2006) The influence of plasma chemical treatments on the activity of the $Li_3Fe_2(PO_4)_3$ catalyst in butanol-2 transformations. Russ J Phys Chem 80:882–885
18. Smiley DL, Davis LJM, Goward GR (2013) An improved understanding of Li^+ hopping pathways and rates in $Li_3Fe_2(PO_4)_3$ using selective inversion ^6Li NMR spectroscopy. J Phys Chem C 117:24181–24188
19. Kim HS, Kim CS (2013) Spin ordering between sub-lattices in nasicon $Li_3Fe_2(PO_4)_3$ measured by Mössbauer spectroscopy. J Appl Phys 113:17E117
20. Shirakawa J, Nakayama M, Wakihara M, Uchimoto Y (2006) Changes in electronic structure upon Li insertion reaction of monoclinic $Li_3Fe_2(PO_4)_3$. J Phys Chem B 110:17743–17750
21. Salah AA, Jozwiak P, Garbarczyk J et al (2005) Local structure and redox energies of lithium phosphates with olivine- and nasicon-like structures. J Power Sources 140:370–375
22. Ivanov-Schitz A (2001) $Li_3Fe_2(PO_4)_3$ solid electrolyte prepared by ultrasonic spray pyrolysis. Solid State Ionics 139:153–157
23. Andersson A (2001) Lithium insertion into rhombohedral $Li_3Fe_2(PO_4)_3$. Solid State Ionics 140:63–70
24. Becht G, Hwu S-J (2006) Hydrothermal ion exchange on submillimeter-size single crystals of a new iron(III) phosphate. Chem Mater 18:4221–4223
25. Yoon Y, Park C, Kim J, Shin D (2012) Characterization of lithium borophosphate glass thin film electrolytes deposited by RF-magnetron sputtering for micro-batteries. Solid State Ionics 225:636–640
26. Nakazawa H, Sano K, Baba M, Kumagai N (2014) Stability of thin-film lithium-ion rechargeable batteries fabricated by sputtering method without heating. J Electrochem Soc 162:A392–A397
27. Bajars G, Kucinskis G, Smits J, Kleperis J (2011) Physical and electrochemical properties of $LiFePO_4$/C thin films deposited by direct current and radiofrequency magnetron sputtering. Solid State Ionics 188:156–159
28. Hamelet S, Gibot P, Casas-Cabanas M et al (2009) The effects of moderate thermal treatments under air on $LiFePO_4$-based nano powders. J Mater Chem 19:3979–3991
29. Yu F, Zhang L, Li Y et al (2014) Mechanism studies of $LiFePO_4$ cathode material: lithiation/delithiation process, electrochemical modification and synthetic reaction. RSC Adv 4:54576–54602
30. Larcher D, Masquelier C, Bonnin D et al (2003) Effect of particle size on lithium intercalation into α-Fe_2O_3. J Electrochem Soc 150:A133–A139
31. Ortiz GF, Hanzu I, Lavela P et al (2010) A novel architectured negative electrode based on titania nanotube and iron oxide nanowire composites for Li-ion microbatteries. J Mater Chem 20:4041–4046
32. Antolini E (2004) $LiCoO_2$: formation, structure, lithium and oxygen nonstoichiometry, electrochemical behaviour and transport properties. Solid State Ionics 170:159–171
33. Yaghoobnejad Asl H, Choudhury A (2014) Phosphorous acid route synthesis of iron tavorite phases, $LiFePO_4(OH)_x F_{1-x}$ [$0 \leq \times \leq 1$] and comparative study of their electrochemical activities. RSC Adv 4:37691–37700
34. Ellis BL, Ramesh TN, Rowan-Weetaluktuk WN et al (2012) Solvothermal synthesis of electroactive lithium iron tavorites and structure of Li_2FePO_4F. J Mater Chem 22:4759–4766
35. Marx N, Croguennec L, Carlier D et al (2010) The structure of tavorite $LiFePO_4(OH)$ from diffraction and GGA + U studies and its preliminary electrochemical characterization. Dalton Trans 39:5108–5116
36. Song J, Cai M-Z, Dong Q-F et al (2009) Structural and electrochemical characterization of SnO_x thin films for Li-ion microbattery. Electrochim Acta 54:2748–2753